

Wearable Device for Daily Continuous Blood Pressure Estimation Based on Pulse Rate Measurement



Toshiyuki Hayase

1 Introduction

Blood pressure is a most basic vital sign, and recently, the importance of the daily continuous blood pressure (DCBP) has been pointed out [1–3]. Studies have been made on the clinical usefulness of ambulatory blood pressure monitoring (ABPM), in which daily blood pressure is automatically measured with a cuff-based portable sphygmomanometer [4–7]. There is also a measurement method called arterial line monitoring in which a catheter is clinically inserted into a blood vessel to measure the blood pressure continuously [8]. This method, however, is not suitable for DCBP measurement because it is highly invasive.

The author proposed a new DCBP estimation method and showed its validity in a previous report [9]. As shown in Fig. 1, the novelty of this method is that a continuous blood pressure estimation is obtained as a solution of the forward problem of a simple model representing the circulatory dynamics and the circulatory control with the input of pulse rate. On the other hand, cuff-type blood pressure measurement [10–12] which is an existing representative noninvasive blood pressure measurement method, and cuffless blood pressure measurement based on pulse waveform [13–18] or pulse propagation time [19–25], obtain the blood pressure as the inverse problem with the input of cuff pressure or pulse waveform. It is difficult to use these existing methods for DCBP measurement devices because of discomfort due to cuff pressure and degradation of measurement accuracy by body movement, respectively. In the previous study, we examined the validity of the proposed method by comparing the analysis results with the measurement results of the automatic sphygmomanometer at 30 min or 1 h intervals for one subject in four days and four subjects in one daytime

T. Hayase (✉)

President-Appointed Extraordinary Professor, Director, Frontier Research Institute for Interdisciplinary Sciences, Tohoku University, 6-3 Aramaki Aza-Aoba, Aoba-Ku, Sendai 980-8578, Japan
e-mail: hayase@fris.tohoku.ac.jp

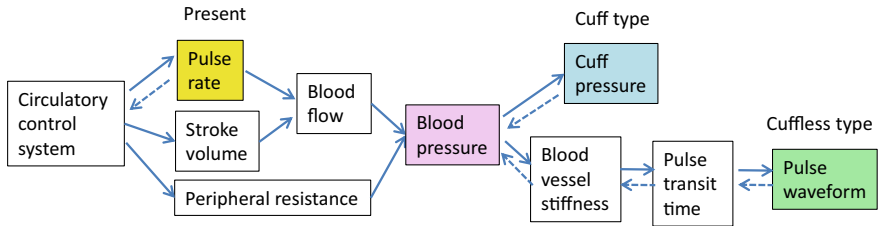


Fig. 1 Principles of blood pressure measurement for the proposed method, conventional cuff type, and cuffless one

[9]. As a result, it was shown that this estimation method gives a reasonable blood pressure estimate.

However, some unresolved problems remained in the previous study. Two parameters of the inverse model of the circulatory control system were determined through a one-parameter optimization problem by applying an empirical constraint for the parameters, the validity of which is not verified yet. Further, the statistical properties of the parameters are unknown since the number of subjects was small. The other two parameters of the circulatory dynamic system model were determined using half of the daily or daytime measurements of the automatic sphygmomanometer, but the effect of the number of measurement data on the parameters is also unknown. In order to apply this estimation method to practical blood pressure estimation devices, it is necessary to solve these problems to clarify the effect of constraints among model parameters and the number of the data of the standard measurement in parameters determination on the accuracy of estimation, realizing good accuracy, small computational load, and small parameter determination measurement number in the estimation method.

In the subsequent article [26], therefore, we focused on the experimental verification and optimization of the continuous blood pressure estimating method. In the article we simultaneously performed a 25-h continuous pulse rate measurement using a commercially available wearable device and blood pressure measurement within 30 min interval using an ABPM device for 29 subjects. Under four conditions for the constraint of model parameters, including the case where two parameters of the inverse model of the circulatory control system are independently changed, blood pressure estimations were performed to determine the optimal parameters and evaluated the estimation error for each condition by comparing the estimation results with the ABPM measurements. From these results, the validity of each condition for the constraint and the statistical properties of the parameters were clarified. Among these conditions, optimum parameter determination method was determined from the viewpoints of accuracy and computational costs. For the optimum parameter determination method of the circulatory control system, the effect of the number of the ABPM data on the accuracy of pressure estimation was investigated and the number of measurement data necessary for appropriate parameter determination was

Fig. 2 Wearable device for **a** pulse rate measurement (<http://www.epson.jp/products/wgps/sf710s/>) and **b** DCBP estimation



obtained. From these results we clarified the applicability of the present estimation method to practical blood pressure estimation devices.

In this article we present this new DCBP estimation method and its experimental validation and optimization based on our former works [9, 26]. First the novel circulatory system model for the present blood pressure estimation with the input of pulse rate is presented in Sect. 2. In the following Sect. 3, we show a computational result for 24 h blood flow dynamics in which values of blood pressure, blood flow, and blood volume in left/right atrium/ventricle and pulmonary/systemic arteries/veins are obtained from pulse rate measurement data with a wearable device (Fig. 2a). Section 4 shows the experimental verification and optimization of the blood pressure estimation method. The blood pressure estimation program was installed in a smart watch (Fig. 2b). The summary of former sections and future expectations are given in Sect. 5.

2 Circulatory System Model

2.1 Introduction

In this section we show the circulatory system model for DCBP estimation. The following model is that of the second article [26], which is practically the same as that of the first report [9]. The circulatory system model consists of the circulatory dynamics model and the circulatory control inverse model. The real circulatory dynamics is a very complex fluid–structure coupled system [27], but the present study models it as a simple lumped parameter dynamical system consisting of eight elastic containers representing a left atrial (1), a left ventricle (2), systemic arteries (3), systemic veins (4), a right atrial (5), a right ventricle (6), pulmonary arteries (7), and pulmonary veins (8); and eight liner resistors connecting these containers (right side of Fig. 3a). The model can be described as basic equations of elastic mechanics

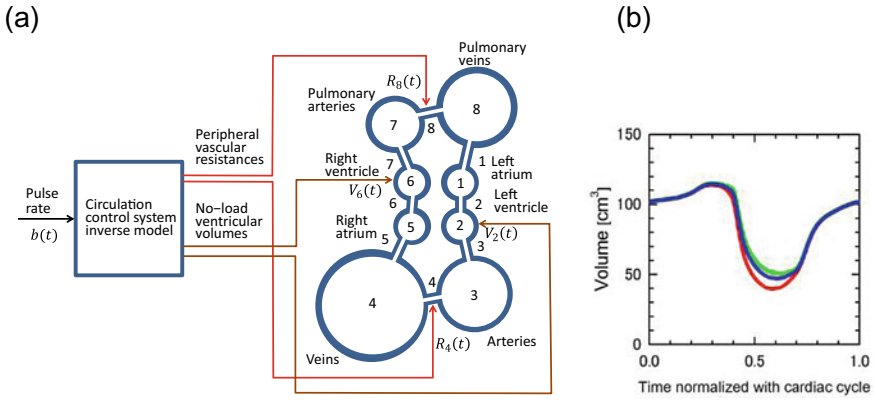


Fig. 3 **a** Circulatory system model consisting of circulatory dynamics model and circulatory control inverse model with the input of pulse rate and **b** variation of ventricular volume by the reference [29] (green), and those at zero pressure, or no-load ventricular volumes, derived from the reference values for left ventricle (red) and right ventricle (blue)

and fluid dynamics, Windkessel model [28], with variables of pressures and volumes of the containers $P_i(t)$ and $V_i(t)$, and flow rates between the containers $Q_i(t)$. Blood flow circulation is generated by introducing the variation of the ventricular volume at zero pressure, or *no-load ventricular volume*, based on the reference [29] to the left and right ventricles (Fig. 3b). Parameters affecting the systemic arterial blood pressure $P_3(t)$ in this circulatory dynamics model is the standard pulse rate b_0 , the elasticity E_{30} and the peripheral resistance coefficient R_{40} of the lumped systemic arteries at the standard pulse rate.

The real circulatory control system is a very complex one including the short-term regulation by the autonomic nervous system and the long-term hormonal regulation, etc. [30], but the present study models it as a simple dynamical model with the input of pulse rate $b(t)$ and the outputs of peripheral vascular resistance of the systemic and pulmonary arteries, $R_4(t)$ and $R_8(t)$, and the no-load ventricular volumes, $V_2(t)$ and $V_6(t)$ (left side of Fig. 3a). The present model represents an inverse system of the real circulatory control system in which the pulse rate is also an output. The circulatory control inverse model is constructed based on the following characteristics: (1) the circulatory control system maintains blood pressure constant, (2) baroreceptors have differential characteristics to effectively respond to short-term changes of blood pressure [31]. (3) the ventricular stroke volume increases with increase of the pulse rate [32]. Parameters of the circulatory control inverse model are the rate s_a of variation of ventricular stroke volumes against the change of the pulse rate (cf. characteristic 3), the rate s_r of variation of peripheral vascular resistances against the change of the low-frequency component of the pulse rate (cf. characteristic 1), and the time constant T_c of the low pass filter characteristics of the control system with the input of the pulse rate (cf. characteristic 2). A total of six parameters of the

present circulatory dynamics and circulatory control inverse models are determined by comparing the measured and calculated blood pressure values.

2.2 Circulatory Dynamics Model

The circulatory dynamics model consists of eight elastic containers representing a left atrial (1), a left ventricle (2), systemic arteries (3), systemic veins including organs (4), a right atrial (5), a right ventricle (6), pulmonary arteries (7), and pulmonary veins (8); and eight liner resistors connecting these containers (Fig. 3a). The numbers assigned to resistors are identical to those of downstream side containers.

Dynamics of the pressures in the containers are represented by the following equations.

$$\frac{dP_i}{dt} = E_i \left(Q_i - Q_{i+1} - \frac{dV_i}{dt} \right) \quad (i = 1, \dots, 8) \quad (1)$$

$V_i(t)$ ($i = 2, 6$) represent the variations of the volume at zero pressure, or *no-load volume*, of the left and right ventricles, respectively, given by

$$V_i(t) = f_i(0) + a(t) \left\{ f_i \left(\frac{b(t)\tau(t)}{b_0\tau_0} \right) - f_i(0) \right\} \quad (i = 2, 6) \quad (2)$$

where $b(t)$ is the pulse rate of the pulse including the time point t , $\tau(t)$ is the elapsed time from the beginning of this pulse, b_0 and τ_0 are the standard pulse rate and the corresponding cardiac cycle, respectively, $f_i(\tau(t)/\tau_0)$ are the variations of the no-load volume of the left and right ventricles for the standard pulse rate derived by reference to the literature [29] (Fig. 3b), $a(t)$, we call it as *no-load stroke volume ratio*, is the ratio of the ventricular volume change to that for the standard pulse rate, determination of the value of which by the circulatory control inverse model will be explained later. No-load volumes of the other containers are constant.

In Eq. (1), E_i ($i = 1 \dots 8$) are the elasticities of the containers. The elasticity of the left ventricle E_2 is assumed to take a relatively lower value for the internal pressure lower than a threshold due to buckling. The elasticity of lumped systemic arteries E_3 is defined as a function of the arterial pressure P_3 considering the characteristics of blood vessels [33]. Refer to the reference for details [9]. Elasticities of the other containers were set constant values for simplicity.

The flow rates Q_i through the resistors are given as

$$Q_i = \frac{C_i(P_{i-1} - P_i)}{R_i} \quad (i = 1 \dots 8) \quad (3)$$

where C_i represent check valve characteristics to prevent reverse flow.

$$C_i = \begin{cases} 0 & P_{i-1} \leq P_i \\ 1 & P_{i-1} > P_i \end{cases} \quad (4)$$

Indices $i = 2, 3, 6, 7$ correspond to the mitral, aortic, tricuspid, and pulmonary valves, respectively. In the other resistors there is no possibility of reverse flow.

R_i ($i = 1 \dots 8$) are the resistance coefficients. Those of the peripheral systemic (4) and pulmonary (8) arteries, respectively, are modeled by the following expression.

$$R_i = R_{i0}r(t)/a(t) \quad (i = 4, 8) \quad (5)$$

where $r(t)$, we call it as *peripheral vascular resistance ratio*, is the ratio of the peripheral vascular resistance coefficient to that for the standard pulse rate multiplied with the no-load stroke volume ratio, determination of the value of which by the circulatory control inverse model will be explained later. The other resistance coefficients are set to constant values.

2.3 Circulatory Control Inverse Model

We explain the models for the no-load stroke volume ratio $a(t)$ and the peripheral vascular resistance ratio $r(t)$ in the followings. Taking into account of the characteristics of the circulatory control system that the ventricular stroke volume increases with increase of the pulse rate [32], the no-load stroke volume ratio $a(t)$ (see Eq. (2)) is modeled by the interpolation of the linear function $a(t) = b(t)/b_0$ of the pulse rate $b(t)$ and the constant $a(t) = 1$ with a weighting factor s_a , we call it as *stroke volume change rate*.

$$a(t) = s_a \frac{b(t)}{b_0} + (1 - s_a) \quad (6)$$

Since the circulatory control system maintains blood pressure constant [30], and baroreceptors have differential characteristics to effectively respond to short-term changes of blood pressure [31], the peripheral vascular resistance ratio $r(t)$ (see Eq. (5)) is modeled as the multiplication of the effects of the lower and higher frequency components of the pulse rate variation.

$$r(t) = r_{LF}(t)r_{HF}(t) \quad (7)$$

where the effect of the lower frequency component of the pulse rate variation $r_{LF}(t)$ is modeled by an inverse function of an interpolation of the linear function $b_{LF}(t)/b_0$ of the lower frequency component of the pulse rate variation $b_{LF}(t)$ and the constant 1 with a weighting factor s_r , we call it as *peripheral resistance change rate* whereas the effect of the higher frequency component of the pulse rate variation $r_{HF}(t)$ is modeled by the inversely proportional function of the pulse rate.

$$r_{LF}(t) = 1/(s_r b_{LF}(t)/b_0 + (1 - s_r)) \quad (8)$$

$$r_{HF}(t) = b_{LF}(t)/b(t) \quad (9)$$

It is noted that in the first paper [9] $r_{LF}(t)$ in Eq. (8) was defined as an interpolation of $b_0/b_{LF}(t)$, inverse function of the low frequency component of the pulse rate change $b_{LF}(t)$, and a constant value of 1. While the previous paper assumed the linearity between the pulse rate change and the peripheral resistance coefficient change, the second article [26] assumes the linearity between the pulse rate change and the peripheral vessel diameter change.

The lower frequency component of the pulse rate variation $b_{LF}(t)$ is expediently modeled by the following second-order low-pass filter with the cut-off frequency of ω_c and the time constant $T_c = 1/\omega_c$, we call it the time constant of slow pulse rate variation.

$$\begin{aligned} \frac{d^2 b_{LF}(t)}{dt^2} + 2\omega_c \frac{db_{LF}(t)}{dt} + \omega_c^2 b_{LF}(t) &= \omega_c^2 b(t) \\ b_{LF}(0) &= b(0) \end{aligned} \quad (10)$$

3 Summary

In this section the circulatory system model for DCBP estimation was presented. The circulatory system model consists of the circulatory dynamics model and the circulatory control inverse model. The real circulatory dynamics is a very complex fluid–structure coupled system, but the present study models it as a simple lumped parameter dynamical system. The real circulatory control system also is a very complex one including the short-term regulation by the autonomic nervous system and the long-term hormonal regulation, etc. [30], but the present study models it as a simple dynamical model with the input of pulse rate and the outputs of peripheral vascular resistance of the systemic and pulmonary arteries, and the no-load ventricular volumes.

4 Analysis Result of Circulatory System

4.1 Introduction

In this section an analysis result of the circulatory system model for DCBP estimation for one subject in one day is presented based on the first paper [9]. The input of the model or the continuous pulse rate variation was measured by a wearable device. Systolic and diastolic pressures and pulse rate were also measured with

the sphygmomanometer with the interval of 30 or 60 min. Differential equations of the model were integrated using the measured pulse rate data. Values of six model parameters were determined for the data by comparing the result of the sphygmomanometer measurement and those of the computations for various combinations of these parameters.

4.2 Methods

Computation

Differential equations for the circulatory dynamics model and the circulatory control inverse model were numerically integrated with the 4-th order Runge–Kutta method. In order to prevent the accumulation of numerical errors, computational results are modified to maintain the total blood volume constant with the interval of one minute of the model time.

Subjects

The subject was a healthy male volunteer of 60 s (subject 1 of the former study [9]). Informed consent was obtained from the subject. The study was approved by the Ethics Committee of Graduate School of Engineering, Tohoku University (15A-9). All research methods were performed in accordance with relevant guidelines and regulations.

Verification Experiments

As the input of the present model, the pulse rate was measured for the subjects by a commercially available wearable device (Wristable GPS, SF-810, EPSON, Japan, Fig. 2a) with the measurement interval of one second in one day. As the purpose of comparison, systolic and diastolic pressures and pulse rate were also measured in sitting position with an automatic sphygmomanometer (HEM-1025, OMRON, Japan) in one day with the interval of 30 min (wake up hours) or 60 min (sleeping hours). Differential equations of the present model were integrated using the measurement data of the pulse rate by the wearable device. The computational time step was fixed to $\Delta t = 0.0002$ s according to preliminary calculations. Calculation was performed by a server (HPCT W215s, Intel Xeon Gold 6132, 2.6 GHz 14 Core \times 2, 192 GB memory, HPC Tec, Japan) with a typical computational time of 370 s for a 24 h calculation. Values of the model parameters were determined for the day by comparing half of the sphygmomanometer measurements and the corresponding computations obtained with various combinations of these parameters. The validity of the present DCBP estimation method was then examined by comparing the other half of measurements and those of DCBP computations with the determined parameters.

Determination of the Optimum Model Parameters

Parameters affecting the systemic arterial blood pressure $P_3(t)$ in this circulatory dynamics model is the standard pulse rate b_0 , the elasticity E_{30} and the peripheral resistance coefficient R_{40} of the lumped systemic arteries at the standard pulse rate. Parameters of the circulatory control inverse model are the stroke volume change rate s_a , the peripheral resistance change rate s_r , and time constant of the slow pulse rate variation T_c . Optimum values of these parameters were determined by comparing the result of the sphygmomanometer measurement and those of the computations for various combinations of these parameters. For detailed explanation refer to Sect. 4.2 or the paper [9].

4.3 Results

We show the results of the subject. Variation of the pulse rate in 24 h in one day is shown in Fig. 4a. Approximate times of activities in the day are, sleeping in 0:00–7:30, wake up in 7:30–24:00, meals at 8:00, 12:00, and 18:30, driving car at 9:00 and 18:00, office work in 10:00–17:30. Measurements of the wearable device (line) and those of the sphygmomanometer (circles) agree well. Differential equations of the present model were integrated using the measurement data of the pulse rate by the wearable device. Values of the model parameters, b_0 , E_{30} , R_{40} , s_a , s_r , and T_c , were determined by comparing the result of the sphygmomanometer measurements and those of the computations performed with various combinations of these parameters. Variations of the no-load ventricular volume ratio $a(t)$ and the peripheral vascular resistance ratio $r(t)$ are shown in Fig. 4b. Computational results for the variations of pressures $P_i(t)$ and volumes $V_i(t)$ of eight elastic containers in the model are shown in Fig. 4c and 4d, respectively. Lines in Fig. 4e show computational results of the daily continuous blood pressure (DCBP) estimation for variation of the systolic (blue), average (red), diastolic (green), and pulse (brown) pressures at all pulses in 24 h obtained from the result of the arterial pressure $P_3(t)$ (Fig. 4c). Circles in the figure are corresponding measurement data by the sphygmomanometer.

In order to obtain the blood pressure estimation at a fixed time point, computation is necessary using pulse rate data in a certain period. According to preliminary calculations, it was confirmed that the computational result in the last 60 s of 120 s calculation starting from the time point 60 s ahead of the target time point using the initial value of the low frequency component of the pulse rate variation evaluated by the data in the period of 1,600 s, which is eight times of the time constant T_c , agreed well with the corresponding results of the 24 h calculation. The average values in the last 60 s were used in the comparison with the measurement data of sphygmomanometer with one minute temporal resolution.

Errors of the computations from measurements of the sphygmomanometer at 40 time points are shown in Fig. 4f for the systolic and diastolic pressures. Colors of the plots correspond to those in Fig. 4e, and closed and cross circles show the data used

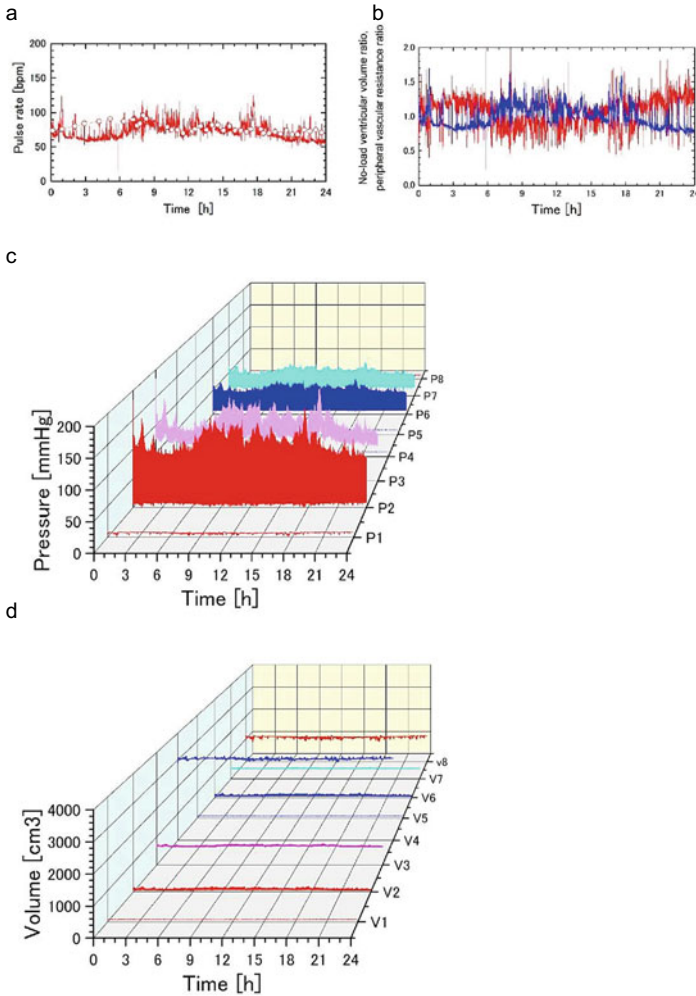


Fig. 4 Daily continuous blood pressure (DCBP) estimation for the subject 1 in the former study [9]. **a** Pulse rate measurements of wearable device (line) and those of sphygmomanometer (circles). **b** Computational results for no-load ventricular volume ratio (blue) and peripheral vascular resistance ratio (red). Pressures (**c**) and volumes (**d**) of eight elastic containers. **e** 24 h computations (lines) and measurements by sphygmomanometer (circles) for systolic (blue), average (red), diastolic (green), and pulse (brown) pressures. Same colors are used in **f–j**. **f** Variation of estimation errors of computations for systolic and diastolic pressures at time points for parameter determination (closed circles) and those for validation (cross circles). **g** Bland–Altman plot showing the relation between errors and averages of estimations and measurements for systolic and diastolic pressures with mean values (middle lines) and mean values $\pm 2 \times$ standard deviation (upper and lower lines) with data for parameter determination data (closed circles, solid lines) and validation data (cross circles, broken lines). **h** Correlation between measurements and calculations for systolic, mean, diastolic, and pulse pressures using the same symbols as those in **g**. Measurements (open circles), corresponding computations (closed circles), and all 24 h computations (light color circles) plotted with pulse rate (**i**) and with low-frequency component of pulse rate (**j**)

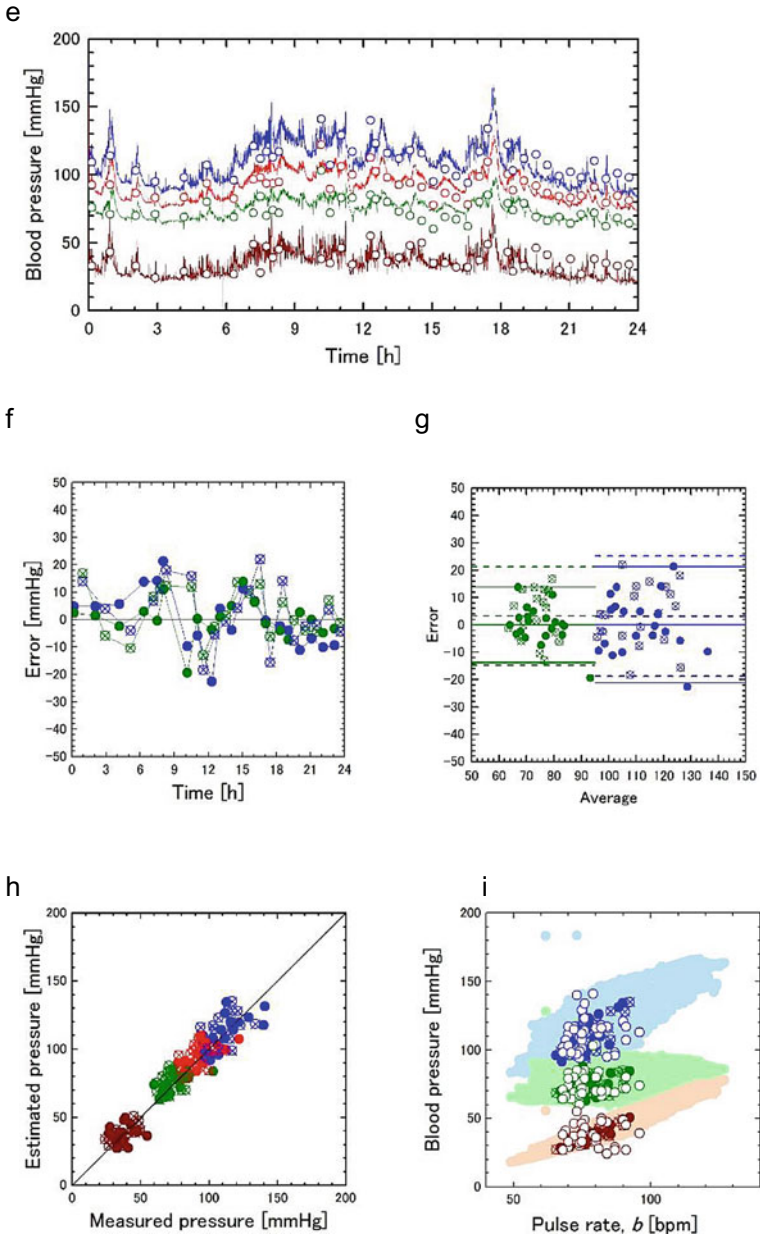
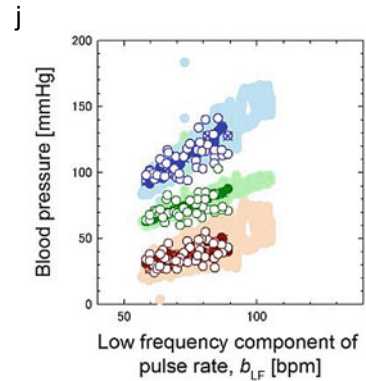


Fig. 4 (continued)

Fig. 4 (continued)



for parameter determination (20 time points) and those for validation (20 time points), respectively. Figure 4g (Bland–Altman plot) shows the relation between errors and averages for estimation and measurement for systolic (blue) and diastolic (green) pressures with mean values (middle lines) and mean values $\pm 2 \times$ standard deviation (upper and lower lines) with data for parameter determination (closed circles, solid lines) and those for validation (cross circles, broken lines). Rows 1–4 in Table 1 show mean values and standard deviations of measurements, estimations, and estimation errors for systolic and diastolic pressures in parameter determination data and those for validation ones.

Correlations between estimations and measurements for systolic (blue), mean (red), diastolic (green), and pulse (brown) pressures are shown in Fig. 4h using the same symbols as those in Fig. 4g. Figure 4i and 4j show the measurements (open circles), corresponding calculations (closed and cross circles), and all the 24 h calculations (light color circles) for the systolic (blue), diastolic (green), and pulse (brown) pressures plotted with the pulse rate and with the low-frequency component of the pulse rate variation, respectively. Rows 5–14 in Table 1 show correlations among measured and estimated blood pressures and pulse rate with Pearson's correlation coefficient r , coefficient of determination R^2 , and slope of regression line. Rows 5–8 correspond to the results in Fig. 4h for parameter determination data and those for validation data. Rows 9–11 and 12–14 correspond to the results for computations and measurements in Fig. 4i and 4j, respectively.

4.4 Discussion

Computational results for systolic, average, diastolic, and pulse pressures for the subject agree with those of measurements with a sphygmomanometer as shown in Fig. 4e and 4h. The computational results for daily variation of systolic pressure show reduced blood pressure in the sleeping hours [4] and fluctuation of the blood pressure in the wake up hours [34] (Fig. 4e). Computational results for the variations

Table 1 DCBP estimation result for the subject in the former study [9]. Rows 1–4 show mean values and standard deviations of measurements, estimations, and estimation errors for systolic and diastolic pressures for parameter determination data and those for validation ones. Following rows show correlations among measured and estimated blood pressures and pulse rate with Pearson’s correlation coefficient r , coefficient of determination R^2 , and slope of regression line. Rows 5–8 correspond to the results in Fig. 4h for parameter determination data and those for validation ones. Rows 9–11 and 12–14 correspond to the results for computations and measurements in Fig. 4i and 4j, respectively

| | | Param. determ. Data | | | Validation data | | |
|---------------------------------------|---------------------|---------------------|----------------|-------|-----------------|----------------|-------|
| | | Meas | Estim | Error | Meas | Estim | Error |
| Systolic | MEAN | 112.0 | 112.6 | 0.0 | 109.4 | 112.0 | 3.2 |
| | SD | 13.3 | 12.6 | 10.6 | 10.9 | 11.8 | 11.0 |
| Diastolic | MEAN | 74.9 | 75.1 | 0.0 | 71.9 | 74.9 | 3.3 |
| | SD | 9.7 | 7.5 | 6.9 | 6.5 | 6.7 | 9.0 |
| Independent variables | Dependent variables | Param. determ. data | | | Validation data | | |
| | | r | R ² | slope | r | R ² | slope |
| Meas. data | P _{sys} | 0.646 | 0.417 | 0.576 | 0.570 | 0.325 | 0.660 |
| | P _{dia} | 0.702 | 0.492 | 0.485 | 0.177 | 0.031 | 0.205 |
| | P _{ave} | 0.713 | 0.509 | 0.588 | 0.440 | 0.194 | 0.551 |
| | P _{pulse} | 0.114 | 0.013 | 0.097 | 0.705 | 0.496 | 0.505 |
| Independent variables | Dependent variables | Estimations | | | Measurements | | |
| | | r | R ² | slope | r | R ² | slope |
| Pulse rate | P _{sys} | 0.635 | 0.403 | 1.173 | 0.083 | 0.007 | 0.145 |
| | P _{dia} | 0.361 | 0.130 | 0.388 | 0.069 | 0.005 | 0.083 |
| | P _{pulse} | 0.878 | 0.771 | 0.785 | 0.057 | 0.003 | 0.062 |
| Low-frequency component of pulse rate | P _{sys} | 0.969 | 0.940 | 1.307 | 0.606 | 0.368 | 0.817 |
| | P _{dia} | 0.997 | 0.994 | 0.782 | 0.454 | 0.206 | 0.420 |
| | P _{pulse} | 0.805 | 0.648 | 0.525 | 0.471 | 0.222 | 0.397 |

of pressures $P_i(t)$ and volumes $V_i(t)$ of eight elastic containers in the model are qualitatively in good agreement with those of the literature [35, 36] (Fig. 4c and 4d). Variation of the no-load ventricular volume ratio $a(t)$ and that of the peripheral vascular resistance ratio $r(t)$ show increase of the no-load ventricular volume and decrease in the peripheral vascular resistance in the systemic and pulmonary arteries with increasing pulse rate through the circulatory control inverse model, respectively (Fig. 4b).

As shown in Table 1, the standard deviation of measurements for the systolic pressure with parameter determination data and that with validation data were 13.3 mmHg and 10.9 mmHg, respectively, and those for the diastolic pressure were 9.7 mmHg and 6.5 mm Hg, respectively. Corresponding values for the errors of computations from measurements were 10.6 mmHg and 11.0 mmHg for the systolic pressure, and those for diastolic pressure were 6.9 mmHg and 9.0 mmHg, respectively, which are

comparable with those of measurements. These standard deviations of the errors are less than 11.3 mmHg, which is evaluated assuming the standard deviation of a common sphygmomanometer (8 mmHg) for those measurements and computations, and independency between them.

$$\sigma_{cal-meas} = \sqrt{\sigma_{cal}^2 + \sigma_{meas}^2} = \sqrt{8^2 + 8^2} = 11.3(\text{mmHg}) \quad (11)$$

Mean value for the errors evaluated with validation data was 3.2 mmHg for the systolic pressure, and that for diastolic pressure was 3.3 mmHg, respectively, which are less than the tolerance of common sphygmomanometers (5 mmHg).

The correlation coefficients and the coefficients of determination have large values to show the effectiveness of the present estimation method as shown in Fig. 4h and rows 5–8 of Table 1. The correlation between the pulse rate and the blood pressure has been considered to be low [37]. As to the measurements and corresponding calculations, correlations with the pulse rate are low as shown in Fig. 4i and rows 9–11 of Table 1, being consistent with former studies. On the other hand, they have significant correlations with the low-frequency component of the pulse rate variation in Fig. 4j and rows 12–14 of Table 1, in accordance with the circadian cycle of the pulse rate [38] and that of the blood pressure [39]. As to all the 24 h calculations, the systolic and diastolic pressures have more significant correlations with the low-frequency component of the pulse rate whereas the pulse pressure has the one with the pulse rate, reflecting the present circulatory control inverse model.

5 Summary

Our results suggest that a fundamental part of DCBP can be represented by continuous pulse rate data and the simple circulatory dynamics and circulatory control inverse model with six model parameters. It is obviously easier to perform DCBP estimation by this method than by the other methods.

Although the present verification is very limited, the mean absolute error was comparable with that of the standard for wearable, cuffless blood pressure measuring devices [40]. Our results demonstrate how DCBP is appropriately estimated by the simple circulatory system model and the pulse rate measurement. We anticipate our methodology to be a starting point of new diagnosis based on DCBP [4–7]. Studies to clarify the relation between DCBP and diseases are important in many clinical departments. Furthermore, present six model parameters can be used as reliable personal vital signs relating the blood pressure, measurement of which often experiences large fluctuations [11].

6 Experimental Validation and Optimization

6.1 Introduction

In this section we show the experimental validation and optimization of the DCBP estimation method based on the second article [26]. We simultaneously performed a 25-h continuous pulse rate measurement using a commercially available wearable device and blood pressure measurement with 30 min interval using an ABPM device for 29 subjects. Under four conditions for the constraint of model parameters, including the case where two parameters of the inverse model of the circulatory control system are independently changed, blood pressure estimations are performed to determine the optimal parameters and evaluate the estimation error for each condition by comparing the estimation results with the ABPM measurements. From these results, the validity of each condition for the constraint and the statistical properties of the parameters are clarified. Among these conditions, optimum parameter determination method is determined from the viewpoints of accuracy and computational costs. For the optimum parameter determination method of the circulatory control system, the effect of the number of the ABPM data on the accuracy of pressure estimation is investigated and the number of measurement data necessary for appropriate parameter determination is obtained. From these results we clarify the applicability of the present estimation method to practical blood pressure estimation devices.

6.2 Method

In this study, we use a circulatory system model of the second article [26] explained in Sect. 2 which is slightly modified from that in the first paper [9] consisting of a circulatory dynamics model and a circulatory control inverse model with the input of pulse rate.

Computations

Differential equations for the circulatory dynamics model and the circulatory control inverse model were numerically integrated with the 4-th order Runge–Kutta method. In order to prevent accumulation of numerical errors, computational results are modified to maintain the total blood volume constant with the interval of one minute of the model time.

Subjects

The subjects were 29 volunteers with an average age of 44 years and a standard deviation of 13 years (Table 2). They are classified to classes 1–3 and none of them to class 4 in the classification of IEEE criteria for cuffless blood pressure measurement devices [40]. Informed consent was obtained from the subjects. The study was approved by

the Ethics Committee of Graduate School of Engineering, Tohoku University (15A-9). All research methods were performed in accordance with relevant guidelines and regulations.

Verification Experiment

We developed a wearable DCBP estimation device (Fig. 2b). A DCBP estimation program based on the algorithm explained in Sect. 2 was installed in a commercially available wearable pulse rate measurement device (M600, POLAR, Sweden), and by specifying model parameters it is possible to perform real-time analysis to display estimated blood pressure. In this study, however, off-line analysis was performed in order to examine the validity of the DCBP estimation method including model parameters determination. As the input of the model, the pulse rate was measured for the subjects by the wearable device with the measurement interval of the pulse period for 25 h from the wake-up time. As the purpose of comparison, systolic and diastolic pressures and pulse rate were also measured in daily life condition with an ambulatory blood pressure (ABP) monitor (TM2433, A&D, Japan) in the above-mentioned time with the interval of 30 min. After the measurement by the wearable device and the ABP monitor, differential equations of the model were integrated using the measurement data of the pulse rate by the wearable device. The computational time step was fixed to $\Delta t = 0.0002$ s according to the former study [9]. Calculation was performed by a server (HPCT W215s, Intel Xeon Gold 6132, 2.6 GHz 14 Core \times 2, 192 GB memory, HPC Tec, Japan) with a typical computational time of 385 s for a 25-h calculation. For each subject, values of the model parameters were determined by comparing half of the ABP monitor measurements and the corresponding computations obtained with various combinations of these parameters. The validity of the present DCBP estimation method was then examined by comparing the other half of the measurements and those of DCBP computations with the determined parameters.

Determination of the Model Parameters

In this study, the model parameters were determined for conditions denoted by Case 1 to Case 4 in Table 3, and the accuracy of blood pressure estimation was investigated

Table 2 Subjects data [26]

| | | |
|--|--------------|------------|
| Total number | | 29 |
| Gender | Male | 26 |
| | Female | 3 |
| Age | MEAN, SD | 43.9, 12.6 |
| | Max, Min | 63, 23 |
| Mean of ABPM measurement for systolic pressure | 1 \leq 119 | 10 |
| | 2 120–139 | 12 |
| | 3 140–160 | 7 |
| | 4 161 \leq | 0 |

for each case. Parameters affecting the systemic arterial blood pressure $P_3(t)$ in this circulatory dynamics model is the standard pulse rate b_0 , the elasticity E_{30} and the peripheral resistance coefficient R_{40} of the lumped systemic arteries at the standard pulse rate. Those of the circulatory control inverse model are the stroke volume change rate s_a , the peripheral resistance change rate s_r , and the time constant of the slow pulse rate variation T_c .

In Case 1, the results of odd number measurements of the ABP monitor in 25 h period (*parameter determination data*) for the systolic and diastolic pressures and the pulse rate, $P_{sysm}(t_n)$, $P_{diam}(t_n)$, $b_m(t_n)$ and quantities derived from these measurement results for the average pressure and the pulse pressure, $P_{avem}(t_n) = (P_{sysm}(t_n) + P_{diam}(t_n))/2$, $P_{pulsem}(t_n) = P_{sysm}(t_n) - P_{diam}(t_n)$, were used to determine above-mentioned model parameters by comparing them with the corresponding results of calculation, $P_{sysc}(t_n)$, $P_{diac}(t_n)$, $b_c(t_n)$, $P_{avec}(t_n)$, and $P_{pulsec}(t_n)$ in the following conditions whereas the results of the even number measurements (*validation data*) were used to verify the validity of the estimation results.

- (1) b_0 is expediently determined as the average value of the pulse rate data in the parameter determination data of the ABP monitor whereas it was determined as the average value of measurement data of the wearable device in 24 h in former study [9].
- (2) E_{30} and R_{40} are determined in the same way as the former study so that the average values of the computation for $P_{pulsec}(t_n)$ and $P_{avec}(t_n)$ are the same as the corresponding results of the measurement. A fixed point iterative method was used for the parameter determination.
- (3) s_a and s_r are determined to minimize the following cost function by multiple conditions that the standard deviation of $P_{pulsec}(t_n)$ and that of $P_{avec}(t_n)$ are the same as the corresponding results of the measurement and that the mean square error of $P_{pulsec}(t_n)$ and thazt of $P_{avec}(t_n)$ are the minimum. The cost function J_{sum} is defined as the weighted sum of two functions corresponding to the above-mentioned conditions. The weighting factor $\alpha = 0.25[\text{Pa}^{-1}]$ was set to the same value as the former study.

Table 3 Definition of cases in verification experiment [26]

| | Case 1 | Case 2 | Case 3 | Case 3 (n) | Case 4 |
|------------------|---|---|------------------------------|------------------------------------|------------------------------|
| s_a, s_r | 2D optimization | 1D optimization | Mean of parameters in Case 2 | Mean of parameters in Case 2 | Mean of parameters in Case 2 |
| E_{30}, R_{40} | 2D optimization | 2D optimization | 2D optimization | 2D optimization using first n data | Mean of parameters in Case 2 |
| b_0 | Mean of ABPM measurement for each subject | Mean of ABPM measurement for each subject | Mean of parameters in Case 2 | Mean of parameters in Case 2 | Mean of parameters in Case 2 |

$$J_{sum} = J_{sd} + \alpha J_{rms} \quad (12)$$

where

$$J_{sd} = (\sigma_{pulsec}/\sigma_{pulsem} - 1)^2 + (\sigma_{avec}/\sigma_{avem} - 1)^2$$

$$J_{rms} = \left[\frac{1}{2N} \sum \left\{ (P_{pulsem}(t_n) - P_{pulsec}(t_n))^2 + (P_{avem}(t_n) - P_{avec}(t_n))^2 \right\} \right]^{1/2} \quad (13)$$

The former function evaluates the degree of agreement for the standard deviations σ_{pulsec} and σ_{avec} of $P_{pulsec}(t_n)$ and $P_{avec}(t_n)$ with those of measurement σ_{pulsem} and σ_{avem} , respectively, and the latter function evaluates the mean square errors of $P_{pulsec}(t_n)$ and $P_{avec}(t_n)$. It is noted that a power of 1/2 was missing in the righthand side of the second formulation of Eq. (13), and the unit of α [Pa^{-1}] in Eq. (12) was incorrectly defined as [Pa^{-2}] in the former study [9]. The parameter determination was performed as a two-dimensional optimization problem; a round-robin method was used to determine the values of s_a and s_r to minimize the cost function in Eq. (12) by changing these parameters between 0 and 1 with the increment of 0.1, respectively.

(4) T_c was set to 200 s which was determined in the former study [9] so that the mean absolute error of $P_{sysc}(t_n)$ and $P_{diac}(t_n)$ is small and the variations of the computed 25 h blood pressure properly represent the characteristics of the measurement.

Other cases are explained in the followings. Case 2, corresponding to the condition of the former study [9], assumes a simpler condition than Case 1 in which the parameter determination was performed as a one-dimensional optimization problem under the empirical constraint of Eq. (14) between two parameters and a round-robin method was used to determine the value of s_r to minimize the cost function in Eq. (12) by changing the parameter between 0 and 1 with the increment of 0.1.

$$s_a = 1 - s_r \quad (14)$$

Case 3 assumes a simpler condition than Case 2 in which values of the parameters s_a , s_r and b_0 are given as the mean values of those of all subjects in Case 2, respectively. Case 3(n) is basically the same as Case 3 but the first n data of the parameter determination data was used for determination of E_{30} and R_{40} . Case 4 assumes the simplest condition in this study in which all the model parameters are constant. In addition to s_a , s_r and b_0 , parameters E_{30} and R_{40} are defined as the mean values of those of all subjects in Case 2, respectively.

From Eqs. (1) and (3), we obtain the approximate expressions of E_{30} and R_{40} by measurement values, P_{sysm} , P_{diam} , and b_m ; and the stroke volume ΔV .

$$E_{30} = (P_{sysm} - P_{diam})/\Delta V$$

$$R_{40} = 60(P_{sysm} + P_{diam})/(2\Delta V b_m) \quad (15)$$

Values of the other model parameters were determined in reference to the literature [35] since their effect on the systemic arterial pressure is relatively low.

6.3 Results

First, the results of Case 1 are shown in the followings. Figure 5a–e and f–i show the model parameters and the mean errors of estimated blood pressure with respect to the validation data of ABPM with the daily average value of systolic pressures measured by ABPM for all 29 subjects, respectively. Figure 5a shows the standard pulse rate b_0 determined as the average value of the pulse rate data in the parameter determination data of ABPM, Fig. 5b, c parameters of the circulatory control inverse model, or the stroke volume change rate s_a and the peripheral resistance change rate s_r , and Fig. 5d, e parameters of the circulatory dynamics model, or the elasticity E_{30} and the peripheral resistance coefficient R_{40} of the lumped systemic arteries at the standard pulse rate b_0 , respectively. Figure 5f, g and h, i show the mean absolute errors for systolic and diastolic pressures, and the mean errors, respectively. Numbers at the plots show the subject numbers, and solid and broken lines show means and means \pm standard deviations, respectively.

DCBP analysis results and measurements with the wearable device and the ABP monitor are compared in Fig. 6 for five subjects corresponding to representative results of Case 1 in Fig. 5. Left figures show measurements of pulse rate by the wearable device (lines) and the ABP monitor (symbols). In the followings, triangles and circles show the parameter determination data and the validation data of ABPM, respectively. Second column figures show daily variations of DCBP for systolic (blue), average (red), diastolic (green), and pulse (brown) pressures by computation (line) and ABP monitor measurement (symbols). Same colors are used in the following results. Third column figures show errors of computed systolic and diastolic pressures with respect to measured ones with ABPM. Fourth figures show correlations between the computations and the measurements for systolic, average, diastolic, and pulse pressures.

Figure 7 shows the correlation between the stroke volume change rate s_a and the peripheral resistance change rate s_r in Case 1 for all 29 subjects. Numbers at symbols show subject numbers, horizontal and vertical solid lines the mean values of s_a and s_r , respectively, and the inclined line is the direction of the first principal component vector of the covariance matrix.

Next, we compare the results of Cases 2–4 with those of Case 1 for all 29 subjects. Figure 8a–e show the relations between the model parameters of Case 1 and those of Cases 2–4 for (a) the standard pulse rate b_0 , (b) the stroke volume change rate s_a , (c) the peripheral resistance change rate s_r , (d) the elasticity E_{30} and (e) the peripheral resistance coefficient R_{40} of the lumped systemic arteries at the standard pulse rate, respectively. Figures 8f–i show the relations between the errors of estimated blood pressure of Case 1 and those of Cases 2–4 for (f, g) the mean absolute errors and (h, i) the mean errors of estimated systolic and diastolic pressures, respectively, with

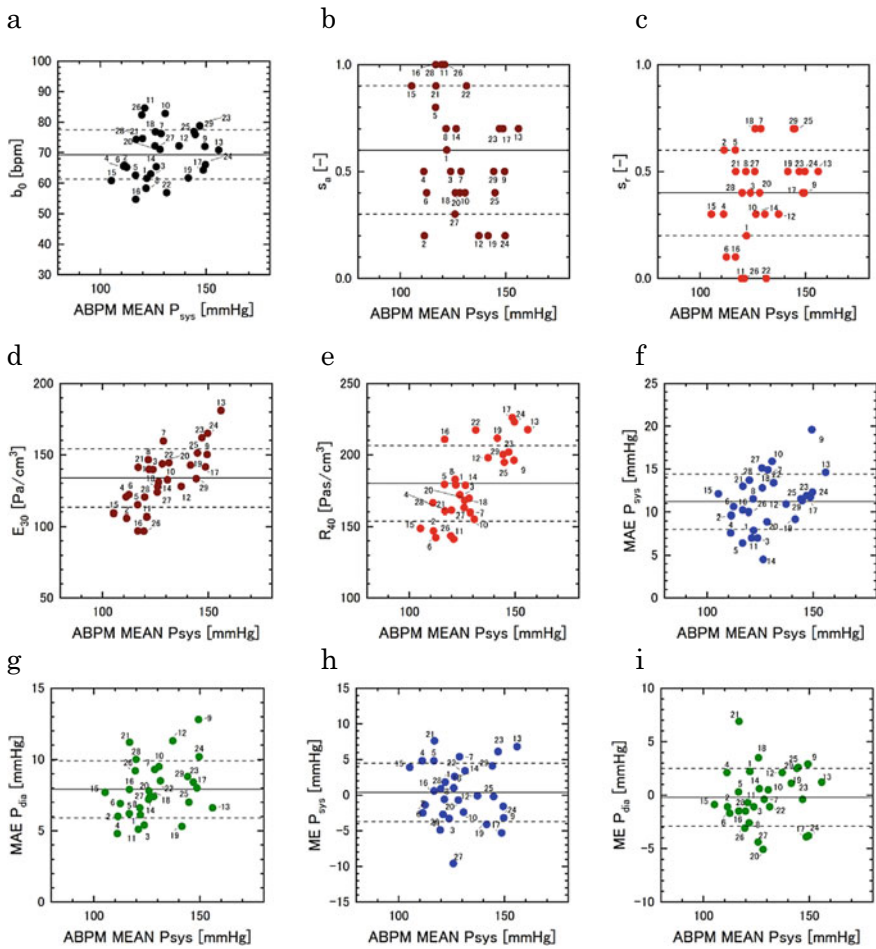
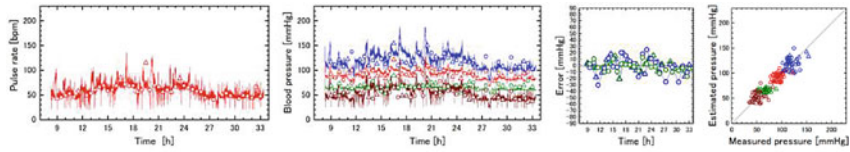
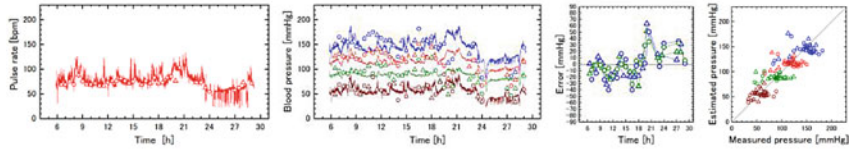


Fig. 5 Analysis results of Case 1. Model parameters and mean errors of estimated blood pressure with respect to the validation data of ABPM are shown with the daily average value of systolic pressure measured by ABPM for all 29 subjects for **a** the standard pulse rate b_0 determined as the average value of the pulse rate data in the parameter determination data of ABPM, **b, c** parameters of the circulatory control inverse model, the stroke volume change rate s_a and the peripheral resistance change rate s_r , **d, e** parameters of the circulatory dynamics model, the elasticity E_{30} and the peripheral resistance coefficient R_{40} of the lumped systemic arteries at the standard pulse rate, **f, g** the mean absolute errors for systolic and diastolic pressures, **h, i** the mean errors. Numbers at the plots show the subject numbers, and solid and broken lines show means and means \pm standard deviations, respectively

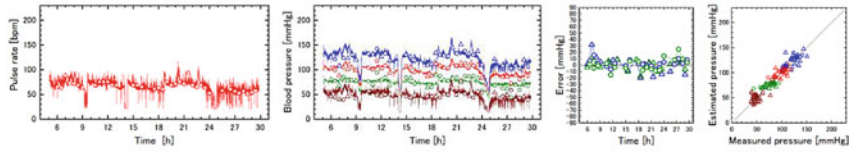
Subject 8



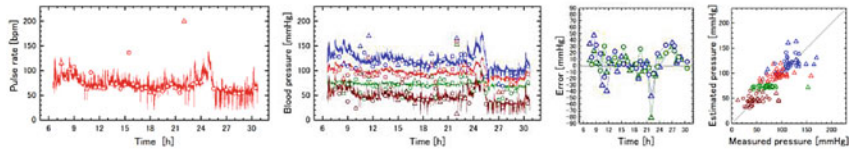
Subject 9



Subject 14



Subject 21



Subject 27

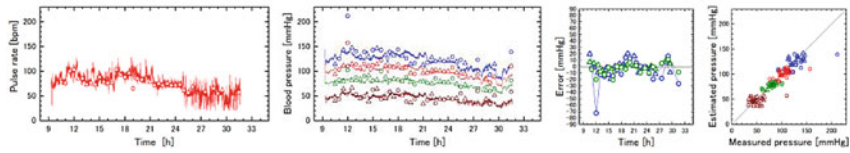
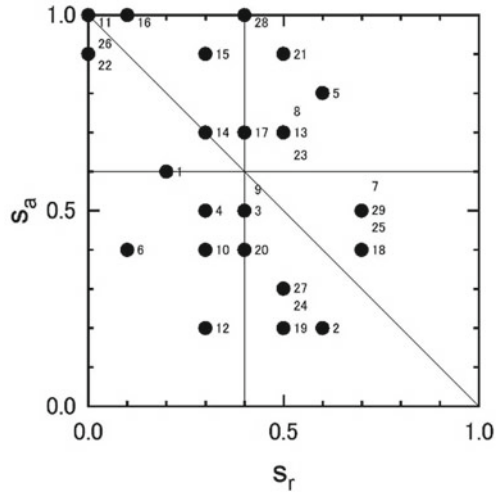


Fig. 6 Comparison among DCBP analysis results and measurements with the wearable device and the ABP monitor for five subjects corresponding to representative results of Case 1 in Fig. 5. First column figures: measurements of pulse rate by the wearable device (lines) and the ABP monitor (symbols). Triangles and circles show the parameter determination data and the validation data of ABPM, respectively. Second column figures: daily variations of DCBP for systolic (blue), average (red), diastolic (green), and pulse (brown) pressures by computation (line) and ABP monitor measurement (symbols). Same colors are used in the following results. Third column figures: errors of computed systolic and diastolic pressures with respect to measured ones with ABPM. Fourth column figures: correlations between computations and measurements for systolic, average, diastolic, and pulse pressures

Fig. 7 Correlation between the stroke volume change rate s_a and the peripheral resistance change rate s_r in Case 1 for all 29 subjects. Numbers at symbols show subject numbers, horizontal and vertical lines the mean values of s_a and s_r , respectively, and the inclined line is the direction of the first principal component vector of the covariance matrix



respect to measurements with ABPM. Results of Cases 2, 3, and 4 are shown by closed, light-colored, and open symbols, respectively. Numbers at the plots show the subject numbers.

Mean values and standard deviations of the model parameters are summarized in Table 4 for Cases 1–4. Those of the mean error, standard deviation, and mean absolute error of estimated systolic and diastolic pressures with respect to the parameter determination data and the validation data, respectively, are in Table 5.

Finally, we show the results of Case 3(n) in which n, the number of the parameter determination data used to determine the circulatory dynamics model parameters, was changed in the condition of Case 3. For all subjects, mean values and standard deviations of the mean absolute errors for the estimated systolic and diastolic pressures with respect to the validation data of ABPM are plotted with the number of the parameter determination data in Fig. 9a and b, respectively. Corresponding results for the mean errors are shown in Fig. 9c and d, respectively. For the purpose of reference in these figures, the results at $n = 0$ show those of Case 4, in which the parameters were determined by averaging those of Case 3 for all the subjects, and the results at $n = 20$ show those of Case 3, in which all parameter determination data were used.

6.4 Discussion

In this study we showed that the continuous blood pressure estimating method based on the simple circulatory system model with the input of pulse rate proposed in the former study [9] can be applied to practical DCBP estimation devices. As the evidence for that, a 25-h continuous pulse rate measurement using a commercially available wearable device and blood pressure measurement with 30 min interval

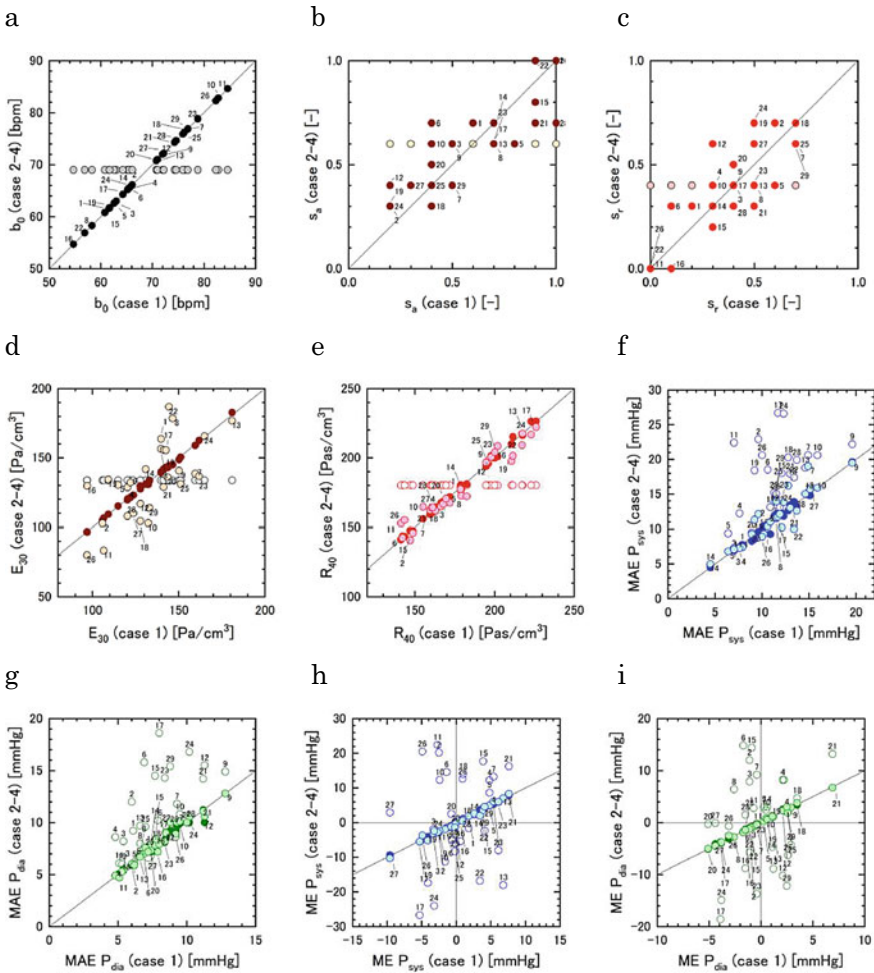


Fig. 8 Comparison of the results of Cases 2–4 with those of Case 1 for all 29 subjects for **a** the standard pulse rate b_0 , **b** the stroke volume change rate s_s , **c** the peripheral resistance change rate s_r , **d** the elasticity E_{30} and **e** the peripheral resistance coefficient R_{40} of the lumped systemic arteries at the standard pulse rate, **f**, **g** the mean absolute errors and **h**, **i** the mean errors of estimated systolic and diastolic pressures, respectively, with respect to measurements with ABPM. Results of Cases 2, 3, 4 are shown by closed, light-colored, and open symbols, respectively. Numbers at the plots show the subject numbers

using an ABPM device were simultaneously performed for 29 subjects. Blood pressure estimations were performed to determine optimal parameters and evaluate the estimation error for each of four conditions for the constraint of model parameters by comparing the estimation results with the ABPM measurements. From these results, the validity of the various conditions of the constraint and the statistical properties of

Table 4 Mean values and standard deviations of the model parameters for Cases 1–4

| | Case 1 | | Case 2 | | Case 3 | | Case 4 | |
|----------------------------------|--------|------|--------|------|--------|------|--------|----|
| | MEAN | SD | MEAN | SD | MEAN | SD | MEAN | SD |
| b_0 [bpm] | 69.4 | 8.1 | 69.4 | 8.1 | 69 | 0 | 69 | 0 |
| E_{30} [Pa/cm ³] | 133.7 | 20.5 | 133.5 | 20.7 | 133.4 | 27.0 | 133.8 | 0 |
| R_{40} [Pa·s/cm ³] | 180.0 | 26.3 | 180.0 | 26.5 | 179.1 | 24.1 | 180.1 | 0 |
| s_a [–] | 0.6 | 0.3 | 0.6 | 0.2 | 0.6 | 0 | 0.6 | 0 |
| s_r [–] | 0.4 | 0.2 | 0.4 | 0.2 | 0.4 | 0 | 0.4 | 0 |
| T_c [s] | 200 | 0 | 200 | 0 | 200 | 0 | 200 | 0 |
| P_{sys0} [mmHg] | 124.5 | 14.3 | 124.6 | 14.4 | 124.2 | 13.6 | 125 | 0 |
| P_{dia0} [mmHg] | 77.6 | 11.4 | 77.8 | 11.4 | 77.4 | 10.1 | 78 | 0 |

Table 5 Mean values and standard deviations of the mean error, standard deviation, and mean absolute error of estimated systolic and diastolic pressures with respect to the parameter determination data and the validation data for Cases 1–4

| | | Case 1 | | Case 2 | | Case 3 | | Case 4 | |
|--------------------------|------|--------|-----|--------|-----|--------|-----|--------|------|
| | | MEAN | SD | MEAN | SD | MEAN | SD | MEAN | SD |
| Estimation errors [mmHg] | | | | | | | | | |
| Systolic | MEAN | 0.0 | 0.1 | 0.0 | 0.1 | 0.0 | 0.1 | 1.2 | 14.2 |
| | SD | 13.5 | 4.4 | 13.6 | 4.5 | 14.6 | 4.8 | 14.8 | 5.0 |
| | MA | 10.4 | 3.2 | 10.4 | 3.2 | 11.2 | 3.4 | 16.6 | 5.3 |
| Diastolic | MEAN | 0.0 | 0.1 | 0.0 | 0.1 | 0.0 | 0.1 | 0.2 | 9.2 |
| | SD | 10.0 | 4.2 | 10.1 | 4.2 | 10.2 | 4.3 | 10.1 | 4.3 |
| | MA | 7.7 | 2.7 | 7.8 | 2.8 | 7.8 | 2.9 | 11.1 | 3.6 |
| Validation errors [mmHg] | | | | | | | | | |
| Systolic | MEAN | 0.4 | 4.1 | 0.4 | 4.2 | 0.3 | 4.3 | 1.4 | 14.1 |
| | SD | 14.0 | 4.3 | 13.9 | 4.3 | 14.5 | 4.7 | 14.6 | 4.8 |
| | MA | 11.2 | 3.2 | 11.2 | 3.3 | 11.6 | 3.6 | 16.4 | 5.8 |
| Diastolic | MEAN | -0.2 | 2.7 | -0.1 | 2.7 | -0.1 | 2.7 | 0.1 | 9.3 |
| | SD | 10.2 | 3.2 | 10.2 | 3.0 | 10.3 | 3.2 | 10.2 | 3.1 |
| | MA | 7.9 | 2.0 | 7.9 | 1.9 | 8.0 | 2.0 | 10.8 | 3.6 |

the parameters were clarified. Among these conditions, optimum parameter determination method was determined from the viewpoints of accuracy and computational costs. For the optimum parameter determination method of the circulatory control system, the effect of the number of the ABPM data on the accuracy of pressure estimation was clarified and the number of measurement data necessary for appropriate parameter determination was clarified. The relations between model parameters and the daily average of systolic pressures by ABPM were clarified for all subjects in Case 1, in which four model parameters were changed independently (Fig. 5a–e).

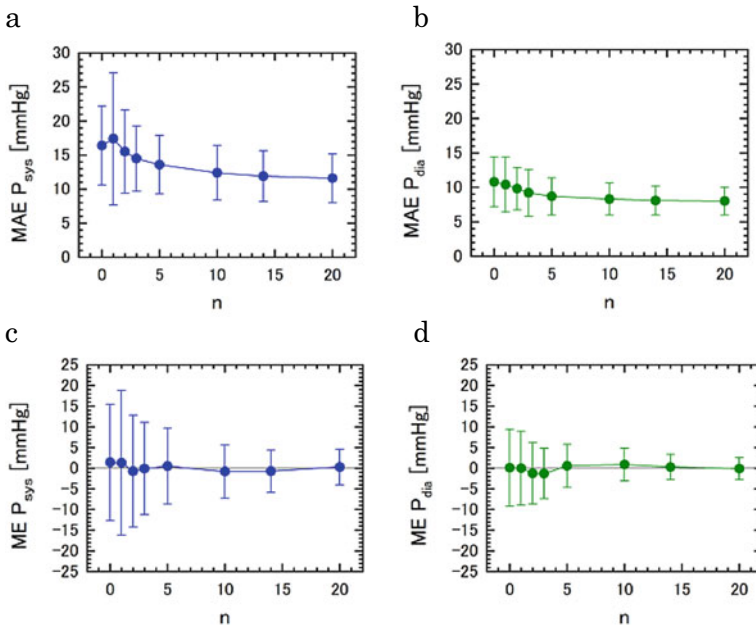


Fig. 9 Results of Case 3(n) for mean values (symbols) and standard deviations (error bars) for all the subjects of **a, b** the mean absolute errors, and **c, d** the mean errors for the estimated systolic and diastolic pressures with respect to the validation data of ABPM, respectively, plotted with the number of the parameter determination data. For the purpose of reference, the results at $n = 0$ show those of Case 4, and the results at $n = 20$ show those of Case 3, respectively

For the stroke volume change rate s_a and the peripheral resistance change rate s_r , no correlation was found to the blood pressure (Fig. 5b, c). In Fig. 7, which shows the correlation between the stroke volume change rate s_a and the peripheral resistance change rate s_r , mean values of both the parameters satisfy Eq. (14), the constraint proposed in the former study, and the direction of the first principal component vector of the covariance matrix agrees with that of Eq. (14), verifying the effectiveness of the constraint. On the other hand, we obtained a physiologically reasonable result that the parameters of the circulatory dynamics model, the elasticity E_{30} and the peripheral resistance coefficient R_{40} of the lumped systemic arteries at the standard pulse rate, respectively, have positive correlations with the blood pressure (Fig. 5d, e). No correlation was found between the standard pulse rate b_0 determined as the average value of the daily pulse rate data in the parameter determination data of ABPM and the blood pressure (Fig. 5a).

Next, we discuss the error of analysis results for all the subjects in Case 1 with respect to the verification data of ABPM. Mean absolute errors and mean errors of systolic and diastolic pressures have no correlation with the blood pressure (Fig. 5 f–i). As to statistical data of estimation errors with respect to validation data of ABPM,

mean errors of systolic and diastolic pressures, $0.4 \pm 4.1/-0.2 \pm 2.7$ mmHg, respectively, were within a standard tolerance of those for common sphygmomanometers, ± 5 mmHg. The standard deviations $14.0 \pm 4.3/10.2 \pm 3.2$ mmHg and mean absolute errors $11.2 \pm 3.2/7.9 \pm 2.0$ mmHg were larger than those for the sphygmomanometers, 8 mmHg and 7 mmHg, respectively. A reason for the larger standard deviations and the mean absolute errors than those of common sphygmomanometer is possibly the errors in the standard validation data. If the errors in the validation data and those in the computation are uncorrelated with zero means and standard deviations of 8 mmHg corresponding to that of common sphygmomanometer, the standard deviation is analytically obtained as Eq. (11) in the former section and the mean absolute error as.

$$E = \sqrt{2(\sigma_{cal}^2 + \sigma_{meas}^2)}/\pi = 9.0(\text{mmHg}) \quad (16)$$

Mean values of standard deviations and mean absolute errors in systolic and diastolic pressures in this study are comparable to those in above expressions.

Next, we discuss five typical analysis results in Case 1 shown in Fig. 6. The result in the top row in the figure for subject 8 is the one the value of the mean absolute error in systolic pressure of which is almost average of those of all subjects (see Fig. 5f). Good agreement is shown in the figures in the top row for the daily variation (second figure), the error (third figure), and the correlation (fourth figure), respectively, between the estimated blood pressures and measured ones with ABPM. On the other hand, the result in the second row for subject 9 is the one the values of mean absolute errors in systolic and diastolic pressures of which are largest, respectively, among those of all subjects. Large error appears around 20 h in the third figure. The result in the third row for subject 14 is the one the value of the mean absolute error in systolic pressure of which is minimum among those of all subjects, and good agreement is shown in the figures. The result in the fourth row for subject 21 and that in the fifth row for subject 27 corresponds to that with the largest mean error in diastolic pressure (Fig. 5i) and that with the negative smallest mean error in systolic pressure (Fig. 5h), respectively. These degradations in accuracy are mostly attributed to the outlier of ABPM data around 22 h and that around 12 h, respectively.

Cases 2–4 are defined by adding several constraints to the parameter determination method in Case 1, resulting in the reduction of the degree of freedom in the method and of the computational load. We discuss the results of these cases by using the plots of the model parameters and the estimation errors of all subjects for each of Cases 2–4 with those of Case 1 (Fig. 8), the statistical data of the model parameters for Cases 1–4 (Table 4), and those of the estimation errors (Table 5). As to the model parameters, values of the stroke volume change rate s_a and those of the peripheral resistance change rate s_r of Case 2 distribute around those of Case 1, and their mean values $s_a = 0.6$ and $s_r = 0.4$ are identical (Fig. 8b, c, Table 4). Values of the elasticity E_{30} of the lumped systemic arteries at the standard pulse rate of Case 2 are close to those of Case 1 although those of Case 3 are far different from those of Case 1 (Fig. 8d, Table 4). Values of the peripheral resistance coefficient R_{40} of the lumped

systemic arteries at the standard pulse rate of Cases 2 and 3 are close to those of Case 1 (Fig. 8e, Table 4). As to the errors with respect to the validation data of ABPM (Fig. 8f–i), Table 5), the results of Case 2 are almost identical to those of Case 1 for all of mean absolute errors and mean errors in systolic and diastolic pressures. In Case 3, the mean absolute errors in systolic pressure in some data deviate from those of Case 1 although the other results are almost identical to those of Case 1. In Case 4, the errors are larger than those of case 1 for most of the results (Fig. 8f–i) with the standard deviations of the mean errors in systolic/diastolic pressures of 14.1/9.3 mmHg (cf. 4.1/2.7 mmHg in Case 1) and the mean values of the mean absolute errors of 16.4/10.8 mmHg (cf. 11.2/7.9 mmHg in Case 1). According to the above discussion, it was revealed that the condition of Case 3, in which the elasticity E_{30} and the peripheral resistance coefficient R_{40} are optimized while the stroke volume change rate s_a and the peripheral resistance change rate s_r are fixed to 0.6 and 0.4, respectively, realizes a blood pressure estimation with an accuracy comparable with that of Case 1 in substantially reduced computational load.

Next, we discuss about the number of ABPM data necessary to determine appropriate values of the elasticity E_{30} and the peripheral resistance coefficient R_{40} in Case 3. Variations of the statistical values of the estimation errors with respect to the number of parameter determination data of ABPM used to determine the model parameters were clarified in Fig. 9 for Case 3(n), in which the first n data were used in parameter determination in Case 3. As to the mean absolute error of the estimated systolic pressure, the mean value and the standard deviation first increase at $n = 1$ from those at $n = 0$, which corresponds to Case 4 with fixed E_{30} and R_{40} , and then monotonically decrease with increasing n to converge to those of Case 3 at $n = 20$ (Fig. 9a). For the mean absolute error of the estimated diastolic pressure, the mean value and the standard deviation almost monotonically decrease with increasing n from those of Case 4 at $n = 0$ to converge to those of Case 3 at $n = 20$ (Fig. 9b). As to the mean errors of the estimated systolic and diastolic pressures, the mean values are close to zero at all values of n in both results, while the standard deviations monotonically decrease to converge to that of Case 3 ($n = 20$) except for the first increase at $n = 1$ for the systolic pressure (Fig. 9c, d). It is confirmed that the accuracy of the estimated blood pressure in Case 3(n) is comparable to that of Case 3 if the number of the data n is set to 10 or larger.

Limitations of this study are discussed in the followings. As to subject groups, this study was performed for volunteer subjects, who were classified into either of groups 1–3 of IEEE standard [40] based on a range of systolic pressure, but not into group 4 which is a hypertension group with a systolic pressure ≥ 161 mmHg. In order to apply the present blood pressure estimation scheme to practical DCBP estimation devices, verification experiments covering all groups 1–4 should be performed in future.

As to variation of the model parameters among days, the former study [9] investigated the variation in five days for one subject. The present study clarified the statistical characteristics of the parameters among subjects but not those among days. Experiment should be performed for sufficient number of subjects in sufficient number of days to clarify the statistics of the parameters among subjects and days.

As to the cost function to determine the model parameters, this study adopted the one in Eq. (12) which is the same as the former study [9], not dealing with the effect of the cost function on the results of blood pressure estimation. Especially, the effect of the weighting factor α in Eq. (12) should be clarified in future.

Concerning improvement of the circulatory system model, it is difficult to evaluate the dynamical characteristics of the model in detail since the validation in this study was done in comparison with ABPM measurement data of 30 min interval, and continuous measurement data are not available. Validation experiment using a continuous blood pressure data obtained with a device such as an arterial line monitoring should be done in future.

In this study the range of parameter determination is limited between 0 and 1 for the stroke volume change rate s_a and the peripheral resistance change rate s_r . As shown in Fig. 5, optimum parameter values are obtained at the boundary of the range as $s_a = 1$ or $s_r = 0$ for five cases in 29 subjects, implying that real optimum values may exist outside the range of $s_a > 1$ or $s_r < 0$. Parameter values in these regions, however, correspond to the computational results with large standard deviations for the pulse pressure or the average pressure, respectively, and are possibly ascribed to outliers in ABPM data. Therefore, it seems reasonable to put above-mentioned limitation in the parameter range.

7 Summary

In this section it was shown that the continuous blood pressure estimating method based on the simple circulatory system model with the input of pulse rate can be applied to practical DCBP estimation devices. A 25-h continuous pulse rate measurement using a wearable device and blood pressure measurement with 30 min interval using an ABPM device were simultaneously performed for 29 subjects. Blood pressure estimations were performed for four conditions modified by adding constraints to model parameters to reduce computational load ranging from Case 1 in which all parameters are changed independently to Case 4 in which all parameters are fixed. Determination of the optimal parameters and evaluation of estimation errors were performed for each of the four conditions by comparing the estimation results with the parameter determination data and the verification data of the ABPM measurement, respectively. Comparison of these results confirmed that the condition of Case 3, in which circulatory dynamics parameters are optimized while the circulatory control system parameters are fixed to the average values of those for all subjects, is suitable for DCBP estimating devices due to comparable accuracy and reduced computational load with respect to those of Case 1. In the results of Case 3, mean values \pm standard deviations of the mean errors for systolic and diastolic pressures were $0.3 \pm 4.3/-0.1 \pm 2.7$ mmHg, and those of the mean absolute errors were $11.6 \pm 3.6/8.0 \pm 2.0$ mmHg, respectively, which were reasonable values taking the errors in the standard validation data of ABPM in consideration. For this condition, circulatory dynamics model parameters can be determined appropriately if about 10 ABPM data

is used for parameter determination. In conclusion, the present estimation method can be applied to practical blood pressure estimation devices with good accuracy, small computational load, and small parameter determination measurement data number.

8 Conclusions

In this article we presented the new DCBP estimation method and its experimental validation and optimization based on our former works [9, 26]. First the circulatory system model with the input of pulse rate for the present blood pressure estimation was presented. The present circulatory system model consists of the circulatory dynamics model and the circulatory control inverse model. The circulatory dynamics model was given as a simple lumped parameter dynamical system. The circulatory control inverse model was defined as a simple dynamical model with the input of pulse rate and the outputs of peripheral vascular resistance of the systemic and pulmonary arteries, and the no-load ventricular volumes.

Next we presented computational result for 24 h blood flow dynamics in which values of blood pressure, blood flow, and blood volume in left/right atrium/ventricle and pulmonary/systemic arteries/veins are obtained from pulse rate measurement data with a wearable device. The results suggest that a fundamental part of DCBP can be represented by continuous pulse rate data and the simple circulatory dynamics and circulatory control inverse model with six model parameters.

Then we discussed the experimental validation and optimization of the DCBP estimation method. A 25-h continuous pulse rate measurement using a wearable device and blood pressure measurement with 30 min interval using an ABPM device were simultaneously performed for 29 subjects. Blood pressure estimations were performed for four conditions modified by adding constraints to model parameters to reduce computational load ranging from Case 1 in which all parameters are changed independently to Case 4 in which all parameters are fixed. Determination of the optimal parameters and evaluation of estimation errors were performed for each of the four. Comparison of these results confirmed that the condition of Case 3, in which circulatory dynamics parameters are optimized while the circulatory control system parameters are fixed to the average values of those for all subjects, is suitable for DCBP estimating devices due to comparable accuracy and reduced computational load. In the results of Case 3, mean values \pm standard deviations of the mean errors for systolic and diastolic pressures were $0.3 \pm 4.3/-0.1 \pm 2.7$ mmHg, and those of the mean absolute errors were $11.6 \pm 3.6/8.0 \pm 2.0$ mmHg, respectively, which were reasonable values taking the errors in the standard validation data of ABPM in consideration. For this condition, circulatory dynamics model parameters can be determined appropriately if about 10 ABPM data are used for parameter determination.

In conclusion, the present estimation method can be applied to practical blood pressure estimation devices with good accuracy, small computational load, and small parameter determination measurement data number.

Acknowledgements This work was supported in part by JST COI Grant Number JPMJCE1303. The author acknowledges Prof. R. Nagatomi of Graduate School of Biomedical Engineering, Tohoku University and Prof. D. Ito of Sendai Seiyō Gakuin University for valuable discussions, Mr. H. Kiso, Mr. A. Sato, Mr. T. Ogasawara for their technical assistance, Mr. O. Iwamoto of Elecom Corp. and Mr. S. Pak for their technical support.

References

1. Andreu-Perez, J., et al.: From wearable sensors to smart implants-toward pervasive and personalized healthcare. *IEEE Trans. Biomed. Eng.* **62**(12), 2750–2762 (2015)
2. Mukkamala, R., et al.: Toward ubiquitous blood pressure monitoring via pulse transit time: theory and practice. *IEEE Trans. Biomed. Eng.* **62**(8), 1879–1901 (2015)
3. Hosanee, M., et al.: Cuffless single-site photoplethysmography for blood pressure monitoring. *J. Clin. Med.* **9**(3) (2020)
4. Staessen, J.A., et al.: Predicting cardiovascular risk using conventional vs ambulatory blood pressure in older patients with systolic hypertension. *Jama-J. Am. Med. Assoc.* **282**(6), 539–546 (1999)
5. Verdecchia, P., et al.: Ambulatory blood-pressure—an independent predictor of prognosis in essential-hypertension. *Hypertension* **24**(6), 793–801 (1994)
6. Anstey, D.E., et al.: Diagnosing masked hypertension using ambulatory blood pressure monitoring, home blood pressure monitoring, or both? *Hypertension* **72**(5), 1200–1207 (2018)
7. Parati, G., et al.: Relationship of 24-hour blood-pressure mean and variability to severity of target-organ damage in hypertension. *J. Hypertens.* **5**(1), 93–98 (1987)
8. Saugel, B., et al.: How to measure blood pressure using an arterial catheter: a systematic 5-step approach. *Critical Care* **24**(1) (2020)
9. Hayase, T.: Blood pressure estimation based on pulse rate variation in a certain period. *Sci. Rep.* **10**(1) (2020)
10. Forouzanfar, M., et al.: Coefficient-free blood pressure estimation based on pulse transit time-cuff pressure dependence. *IEEE Trans. Biomed. Eng.* **60**(7), 1814–1824 (2013)
11. Pickering, T.G., et al.: Recommendations for blood pressure measurement in humans and experimental animals—part 1: blood pressure measurement in humans—a statement for professionals from the subcommittee of professional and public education of the American heart association council on high blood pressure research. *Hypertension* **45**(1), 142–161 (2005)
12. Verberk, W.J., et al.: Home blood pressure measurement—a systematic review. *J. Am. Coll. Cardiol.* **46**(5), 743–751 (2005)
13. Chandrasekhar, A., et al.: An iPhone application for blood pressure monitoring via the oscillometric finger pressing method. *Sci. Rep.* **8** (2018)
14. Chandrasekhar, A., et al.: Formulas to explain popular oscillometric blood pressure estimation algorithms. *Front. Physiol.* **10** (2019)
15. Peng, R.C., et al.: Cuffless and continuous blood pressure estimation from the heart sound signals. *Sensors* **15**(9), 23653–23666 (2015)
16. Suzuki, A.: Inverse-model-based cuffless blood pressure estimation using a single photoplethysmography sensor. *Proc. Inst. Mech. Eng. Part H-J. Eng. Med.* **229**(7), 499–505 (2015)
17. Kachuee, M., et al.: Cuffless blood pressure estimation algorithms for continuous health-care monitoring. *IEEE Trans. Biomed. Eng.* **64**(4), 859–869 (2017)
18. Chandrasekhar, A., et al.: PPG sensor contact pressure should be taken into account for cuff-less blood pressure measurement. *IEEE Trans. Biomed. Eng.* **67**(11), 3134–3140 (2020)
19. Ding, X.R., et al.: Continuous cuffless blood pressure estimation using pulse transit time and photoplethysmogram intensity ratio. *IEEE Trans. Biomed. Eng.* **63**(5), 964–972 (2016)

20. Huynh, T.H., Jafari, R., Chung, W.Y.: Noninvasive cuffless blood pressure estimation using pulse transit time and impedance plethysmography. *IEEE Trans. Biomed. Eng.* **66**(4), 967–976 (2019)
21. Ma, Y.J., et al.: Relation between blood pressure and pulse wave velocity for human arteries. *Proc. Natl. Acad. Sci. U.S.A.* **115**(44), 11144–11149 (2018)
22. Mase, M., et al.: Feasibility of cuff-free measurement of systolic and diastolic arterial blood pressure. *J. Electrocardiol.* **44**(2), 201–207 (2011)
23. Sharma, M., et al.: Cuff-less and continuous blood pressure monitoring: a methodological review. *Technologies* **5**(2) (2017)
24. Wong, M.Y.M., Poon, C.C.Y., Zhang, Y.T.: An evaluation of the cuffless blood pressure estimation based on pulse transit time technique: a half year study on normotensive subjects. *Cardiovasc. Eng.* **9**(1), 32–38 (2009)
25. Yavarimanesh, M., et al.: Commentary: relation between blood pressure and pulse wave velocity for human arteries. *Front. Physiol.* **10** (2019)
26. Hayase, T.: Yamada, I. (ed.) Development of Blood Flow Dynamics Sensing Device, in *Smart Healthcare*, pp. 217–229. NTS publishing, Tokyo (2023) (in Japanese)
27. Lu, K., et al.: Cerebral autoregulation and gas exchange studied using a human cardiopulmonary model. *Am. J. Physiol.-Hear. Circ. Physiol.* **286**(2), H584–H601 (2004)
28. Shi, Y.B., Lawford, P., Hose, R.: Review of zero-D and 1-D models of blood flow in the cardiovascular system. *Biomed. Eng. Online* **10** (2011)
29. Klabunde, R.E.: *Cardiovascular Physiology Concepts*, 2nd edn., xi, 243 p. Lippincott Williams & Wilkins/Wolters Kluwer, Philadelphia, PA (2012)
30. Sun, M.K.: Central neural organization and control of sympathetic nervous system in mammals. *Prog. Neurobiol.* **47**(3), 157–233 (1995)
31. Malpas, S.C., Ninomiya, I.: THE AMPLITUDE AND PERIODICITY OF SYNCHRONIZED RENAL SYMPATHETIC-NERVE DISCHARGES IN ANESTHETIZED CATS - DIFFERENTIAL EFFECT OF BARORECEPTOR ACTIVITY. *J. Auton. Nerv. Syst.* **40**(3), 189–198 (1992)
32. Weissler, A.M., Peeler, R.G., Roehll, W.H.: Relationships between left ventricular ejection time, stroke volume, and heart rate in normal individuals and patients with cardiovascular disease. *Am. Heart J.* **62**(3), 367–370 (1961)
33. Hayashi, K., et al.: Clinical assessment of arterial stiffness with cardio-ankle vascular index: theory and applications. *J. Hypertens.* **33**(9), 1742–1757 (2015)
34. Hayashi, T., et al.: Seasonal influence on blood pressure in elderly normotensive subjects. *Hypertens. Res.* **31**(3), 569–574 (2008)
35. Cooney, D.O.: *Biomedical engineering principles : an introduction to fluid, heat, and mass transport processes*. In: *Biomedical Engineering and Instrumentation Series*, vol. 2, xvi, 458 p. M. Dekker, New York (1976)
36. Ugander, M., Jense, E., Arheden, H.: Pulmonary intravascular blood volume changes through the cardiac cycle in healthy volunteers studied by cardiovascular magnetic resonance measurements of arterial and venous flow. *J. Cardiovasc. Magn. Reson.* **11** (2009)
37. Cohen, Z., Haxha, S.: Optical-based sensor prototype for continuous monitoring of the blood pressure. *IEEE Sens. J.* **17**(13), 4258–4268 (2017)
38. Weibel, L., et al.: Comparative effect of night and daytime sleep on the 24-hour cortisol secretory profile. *Sleep* **18**(7), 549–556 (1995)
39. Shea, S.A., et al.: Existence of an endogenous circadian blood pressure rhythm in humans that peaks in the evening. *Circ. Res.* **108**(8), 980–U207 (2011)
40. IEEE Standard for Wearable, Cuffless Blood Pressure Measuring Devices. *IEEE Std.*, pp. 1708–2014. New York, USA (2014)